The International Journal of Advanced Manufacturing Technology (2018) 97:3963–3980
https://doi.org/10.1007/s00170-018-2230-4

ORIGINAL ARTICLE

Exploring the use of two servo-valves for servo-pneumatic control

Paul Dólleman[1] · João Falcão Carneiro[2] · Fernando Gomes de Almeida[2]

Received: 16 March 2018 / Accepted: 22 May 2018 / Published online: 5 June 2018

Abstract

Pneumatic actuators find widespread use in industry when motion between two end-points is required, given their high power to weight ratio and low maintenance requirements. However, classical PID control of pneumatic actuators may present several undesired features, such as large steady-state errors. In this work, a two servo-valve architecture was developed for the position control of a servo-pneumatic system. With this architecture, the two servo-valves are independently controlled—the one connected to the charging chamber is controlled so as to maintain an approximately constant pressure in the discharging chamber, while the other handles motion control. The use of this control architecture is justified through analysis of the system model. By using this architecture with linear PID-family controllers, the aim is to enhance motion smoothness and improve the steady-state errors usually obtained with PID controllers in classical architectures, where the control actions are applied symmetrically to each servo-valve. Both simulation and experimental results show that the newly developed architecture compares very favorably to the classical one in terms of motion smoothness, steady-state positioning errors, and robustness to load variations.

Keywords Servo-pneumatic systems · Linear control systems · PID control · Servo-pneumatic motion control

Nomenclature

$A_{A,B}$	Piston area in chamber A,B (m^2)
A_r	Cross-sectional area of the rod (m^2)
A_q	Heat-transfer area of the actuator chamber (m^2)
C_i	Sonic conductance of orifice i (m^3 Pa^{-1} s^{-1})
c_p	Specific heat for constant pressure (J kg^{-1} K^{-1})
c_v	Specific heat for constant volume (J kg^{-1} K^{-1})
ε	Error
ε_p	Pressure error (Pa)
ε_{ss}	Steady-state positioning error (m)
ε_x	Positioning error (m)
F	Force (N)
F_{ext}	External force (N)
F_{fr}	Friction force (N)
K_d	Proportional acceleration gain (V m^{-1} s^{-2})
K_{vel}	Proportional velocity gain (V m^{-1} s)
K_{ep}	Proportional ε_{pdch} gain (V Pa^{-1})
K_p	Proportional pressure gain (Discharging Chamber) (V Pa^{-1})
K_{pos}	Proportional positioning gain (V m^{-1})
K_{pr}	Proportional pressure gain (Charging Chamber) (V Pa^{-1})
K_v	Reference velocity feed-forward gain (V m^{-1} s)
λ_0	Equilibrium heat transfer coefficient (W m^{-2} K^{-1})
$\dot{m}$	Mass flow rate (kg s^{-1})
$\dot{m}_{A,B}$	Mass flow rate entering/exiting chambers A,B (kg s^{-1})
$\dot{m}_{A1,A2,B1,B2}$	Mass flow rate through restriction 1,2 of servo-valve A,B (kg s^{-1})
m	Payload Mass (kg)
n	Polytropic index
ρ	Density (kg m^{-3})
$p_{A,B}$	Pressure in chamber A,B (Pa)
$p_{ui,di}$	Upstream/downstream pressure in orifice i (Pa)
p_{atm}	Atmospheric pressure (1 bar)
p_{dch}	Pressure in the discharging chamber (Pa)
p_{ref}	Pressure reference in the discharging chamber (Pa)

✉ João Falcão Carneiro
jpbrfc@fe.up.pt

[1] INEGI, Universidade do Porto, Rua Dr. Roberto Frias, s/n, 4200-465 Porto, Portugal

[2] INEGI, Faculdade de Engenharia, Universidade do Porto, Rua Dr. Roberto Frias, s/n, 4200-465 Porto, Portugal

p_s	Source pressure (7 bar)
R	Specific gas constant for air (ideal gas) (J kg^{-1} K^{-1})
r	Critical pressure ratio
$R_{1,2}$	Restriction 1,2 of a servo-valve
$T_{A,B}$	Temperature in chamber A,B (K)
T_{amb}	Ambient air temperature (K)
T_a	Anti-windup parameter (reset time) (s)
T_{aCl}	Anti-windup parameter (reset time) in classical PID (s)
T_{ip}	Integrator time in the pressure controller (s)
T_{iCl}	Integrator time in the classical PID controller (s)
T_s	Supply air temperature (K)
$u_{A,B}$	Control action applied to servo-valve A,B (V)
x	Position (m)
x_{ref}	Position reference (m)
$\dot{x}$	Velocity (m s^{-1})
$\dot{x}_{ref}$	Velocity reference (m s^{-1})
$\dot{x}_{est}$	Estimated velocity (m s^{-1})
$\ddot{x}$	Acceleration (m s^{-2})
$\ddot{x}_{est}$	Estimated acceleration (m s^{-2})

1 Introduction

Pneumatic actuation systems find widespread use throughout many industries, as they represent a mature, simple, and readily available technology. These systems are economical, robust, and compact, often being a competitive option for simple motion tasks involving mid-ranged speed and force. They rival DC servomotors in those applications, having the advantage of a higher power-to-weight ratio and the absence of heat or magnetic field generation. Furthermore, pneumatic systems are clean and low-maintenance, while also having a simple mechanical construction. These features make them a viable choice for specific applications such as wafer positioning devices [1], robotic surgery in MRI environments [2], haptic devices [3], or exoskeletons [4].

There are, however, some disadvantages to the use of pneumatic systems. Besides the low energy efficiency inherent to the use of compressed air, the highly non-linear behavior of these systems (due to phenomena like friction) makes them difficult to model and control and, consequently, unsuitable for more complex control tasks involving smooth motion and accurate positioning. In order to tackle this problem, researchers all over the world have been developing, in recent years, advanced models and non-linear control strategies. Modeling studies are typically focused on the evolution of air pressure inside the actuator chambers [5, 6], servo-valve models [7, 8], and on the accurate description of the friction force on the actuator seals [9, 10]. Furthermore, several studies can be found on the development of parameter identification techniques for servo-pneumatic models [11–13]. Regarding control strategies, it has been shown that it is possible, given the right control architecture, to achieve high-accuracy motion control both in positioning [14] and trajectory following tasks [15]. The authors were able to achieve a control positioning error of ± 5 μm, when arbitrarily positioning a piston of an actuator with 280 mm stroke length, and for payloads varying from 2.7 to 13 kg, therefore showing robustness. More recently, using an enhanced version of the controller developed in [15], the authors were able to obtain even better results in the micrometer range [16]. In fact, the control positioning error was limited only by the encoder resolution (1 μm), independently of the target position, for loads of 3 and 8 kg, and with no controller re-tuning whatsoever.

The latest related published work by the same authors presented a controller architecture that included separate motion and pneumatic force controllers—the motion controller is based on integral sliding mode, while the force controller is based on a non-linear state feedback approach. The steady-state errors were shown to be under 50 μm [17]. Even though these are higher than the previously mentioned values, the control law proved to be rather robust, withstanding a five-fold payload variation and, more importantly, maintaining good performance in the absence of a friction model.

Other non-linear approaches include the work in [18], wherein the authors designed a multiple-input single-output non-linear position control law using a backstepping methodology. This resulted in maximum steady-state errors of ± 0.05 mm for a 9.5-mm bore cylinder and 1.5 kg moving mass.

A relevant topic within this framework lies in the use of two servo-valves instead of one. Some of the previously mentioned studies use this configuration, but typically, servo-pneumatic systems use one five-orifice servo-valve to modulate the amount of air entering or exiting both cylinder chambers. Since there is only one spool, it is not possible to independently modulate the airflow through each working orifice. This means that the pressure dynamics of the two chambers are coupled in a manner that is dependent on the system state and also on the particular dimensions and characteristics of the servo-valves and actuator.

One important system property for pneumatic motion control is the pneumatic stiffness, and this is a property that can vary significantly with the system state, due to the already mentioned coupling of the pressure dynamics when using one servo-valve. The pneumatic stiffness is dependent on the piston position and pneumatic force inside each chamber [19], and so, when using only one servo-valve, it is also velocity-dependent [20]. As shown in the aforementioned work, this drawback can be very pronounced around zero velocity. This dependency is highly undesirable for control purposes, since sudden changes in the system's inherent bandwidth characteristics must be accounted for by

the controller. A two servo-valve architecture can surpass this drawback, enabling a decoupling of pressure dynamics and independent force control in each chamber [20]. The particular approach presented in that work was developed for pneumatic force controllers, but it can be used as part of a cascaded motion controller—it is expected that such a controller would present improved smoothness of movement, since pneumatic force variations would be kept under control.

In [21], the authors used two servo-valves and a sliding mode approach, defining two sliding surfaces—one for the position of the piston and the other for the pressure of the charging chamber. There are therefore two subsystems, one for motion control and the other for pressure control. This is similar to what is studied in this paper, with the notable differences that in the present case, linear controllers are used (as opposed to sliding mode controllers), and while in [21], the control architecture allows for pressure control solely in the main chamber; in the present study, both chambers' pressures are controlled, depending on the direction of motion. Also, the aim of the pressure control-loop was to minimize energy consumption, while this paper presents pressure regulation as a means to improve motion smoothness through choked flow conditions. The aforementioned architecture further allowed the authors to choose the pressure of the main chamber for a given motion trajectory. In terms of results, positioning errors of approximately 0.2 mm were obtained, with the high control activity usually expected from sliding mode approaches. In a more recent study [22], the authors compared different control laws in the control of an electro-pneumatic system comprising two servo-valves. The performance of two higher-order SMCs (HOSMCs) was assessed. One was a SISO (single input single output), where the output was the piston position and the input was symmetrically applied to each servo-valve. The other was a MIMO (multiple input multiple output), with the output variables being the piston position and the pressure in one of the chambers—this architecture, along with the use of two servo-valves, enables an improvement regarding the already discussed pneumatic stiffness of the system. The SISO controlled system showed positioning errors of several tens of micrometers, depending on the position reference and payload. The MIMO controlled system showed even better results, with positioning errors of few tens of micrometers. Even though HOSMCs typically reduce chattering, the MIMO still presented significant levels of control activity.

Notice that all these results were obtained using non-linear approaches. It is a known fact that, in servo-pneumatics, non-linear controllers typically present much better results than their linear PID counter-parts in a single-degree-of-freedom configuration ($u_A = -u_B$). However, they require a more complex design process and may be difficult to implement and tune. With SMCs, a frequent approach in non-linear control for servo-pneumatics, there is also the issue of the *chattering* phenomenon—even with smoothing strategies like boundary layers [23], this approach may present too much high-frequency control activity, which is to be avoided if smoothness of movement is an important requirement.

Linear and PID-based approaches have also been successful in achieving satisfactory motion control. Ning and Bone [24] used a state-feedback approach with a friction compensation method and were able to obtain a steady-state positioning accuracy of ± 0.01 mm, although the dynamic performance and specifically the final approach to the reference position presented some minor problems. This was for both vertical and horizontal movements and for payloads ranging from 0.3 to 11.3 kg, without re-tuning the controller. Fok and Ong [25] used an experimentally tuned PD controller to position a 40-mm bore size and 1.8-m stroke length rodless cylinder. Positioning errors of ± 0.3 mm were obtained, in all five piston position references, for both 60- and 80-kg payloads. PID control has also been successfully implemented with various modifications. In the work by [26], the authors developed a PID controller with friction compensation and a stabilization algorithm, where the controller gains are adapted by means of fuzzy logic. This resulted in steady-state positioning errors of around 0.5 mm, with robustness to air supply pressure variations. In [27], a self-regulating non-linear PID control law was designed, which was able to guarantee steady-state positioning errors of 0.01 mm for step-inputs with 400-mm amplitude, and for loads of 3.2–28 kg, showing high robustness. In [12], the authors designed a cascaded PID controller for position (outer loop) and velocity (inner loop) control of a servo-pneumatic system. The controller gains were found by Particle Swarm Optimization (PSO) tuning, using the sum of squared errors (SSE) of the position as a criterion function. Results showed that the PSO-tuned controller had a better and faster transient response than its self-tuned counterpart, and presented a maximum steady-state positioning error of 0.5 mm.

Speaking in a broader sense, PID controllers in general have the advantage of being a widespread, tried-and-proven solution that has been extensively studied - PID controllers and their variations make up a large percentage of all industrial controllers, and play important roles in widely different applications outside of servo-pneumatics, such as the control of active automobile suspension systems [28] or of continuously stirred tank reactors (CSTRs) [29]. Furthermore, PID controllers often do not require a system model for satisfactory performance (as this work will show), which adds to the simplicity of their implementation. In fact, in the frequently used approach of model-based control design, important issues may arise with the use

of system identification techniques to determine system parameters. Experimental measurements are typically prone to noise and other disturbances, and so the selection of the parameter identification algorithm must be a careful one—the effect of the aforementioned measurement noise (often non-Gaussian) on the convergence and stability of a solution should therefore be minimized through the use of robust identification techniques [30–32].

The results that have been presented often show errors in the range of tens or hundreds of micrometers, providing a general idea of the possibilities in accurate motion control of pneumatic systems. It seems that sliding-mode approaches result in the lowest positioning errors, with the added advantage of robustness in the face of uncertainties and payload variations. This, however, comes at the cost of excess control activity and difficulties in achieving smooth motion. This paper presents a control architecture which avoids the sliding mode approach and instead focuses on linear PID-family controllers and the use of two servo-valves. One, connected to the actuator's charging chamber, will be controlled in a way that guarantees approximately constant pressure in the discharging chamber, where the other servo-valve will be controlled so as to guarantee the fulfillment of motion specifications. This additional degree of freedom provided by the second servo-valve allows us to not only have a motion controller but also a pressure regulator, in order to maintain an approximately constant pressure in the discharging chamber. The main reason for having this pressure regulation is motion smoothness, since, as will be shown through analysis of the system model, a constant pressure of the right value in the discharging chamber will essentially guarantee choked flow. Choked flow conditions remove the influence of the pressure differential on the volumetric flow rate, which in turn defines piston velocity. The result is therefore a sort of meter-out configuration with, ideally, constant pressure and choked flow—this combination of factors should significantly contribute to an improvement in motion smoothness. To the best of the authors' knowledge, this is the first published work following an approach where two independent servo-valves are used to control both motion and pressure for the purposes of motion smoothness, by exploiting the thermodynamic characteristics of choked flow. In the most similar approach found [21], motion and pressure controllers' control actions are allocated to the same chamber—no switching exists, and pressure regulation is mainly performed with energy saving purposes.

The developed controller was experimentally tuned, but it should nevertheless be highlighted that methods in the literature exist which employ specific algorithms in an automatic search for optimal control parameters. As an example, in [33, 34] the authors successfully use metaheuristic (nature inspired) algorithms to find the controller parameters.

This paper is comprised of five sections. The following section features a brief presentation of the experimental set-up and the mathematical model by which it is simulated, and an important characteristic of the system is briefly studied: the coupling of the dynamics of pressure and velocity. Section 3 is dedicated to control design, including the implementation of a controller switching strategy, since the servo-valves switch roles for forward and backward movements. Section 4 is used to present both experimental and simulation results, and finally, Section 5 features the main conclusions that can be drawn from this work.

2 Analysis of the system model

2.1 Experimental setup

A picture of the experimental setup can be seen in Fig. 1.

The servo-pneumatic system comprises a linear actuator driving a payload, two servo-valves, a digital encoder used to measure position with a 1 μm resolution and two pressure transducers used to provide the pressure values inside the actuator chambers. The data acquisition system has a 1 kHz sampling frequency. The position data is fed into a Kalman filter used to estimate velocity and acceleration. The discrete Kalman filter follows a simple concept: it produces an estimate of the system state based on the system model, and then corrects that estimate based on new measurements, i.e. the algorithm features two steps—estimation and correction. See [35] for the detailed design of the Kalman filter used in this work, along with results that show how it performs better than other estimation methods.

The pneumatic linear actuator is manufactured by ASCO-Numatics and has a stroke length of $l = 240$ mm, a piston diameter of $\phi_p = 32$ mm and a rod diameter

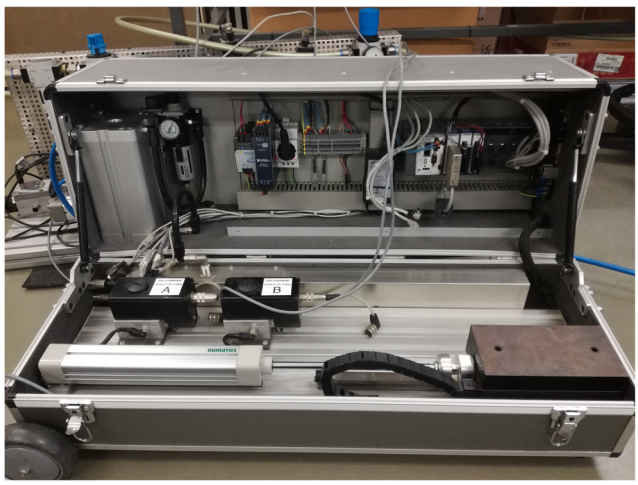

Fig. 1 Experimental setup

of $\phi_r = 12$ mm. The two three-way servo-valves are ASCO-Joucomatic SENTRONICs, which have a command voltage of [−10 10] V, a bandwidth of approximately 100 Hz and a nominal maximum mass flow rate of 1200 SLPM. For a detailed description of the data acquisition hardware and software, see [16]. For simulation purposes, both the quantization of the position readings due to the encoder resolution and the time-discretization due to the sampling frequency are taken into account. Electrical noise in the pressure readings is also modeled according to experimental noise data. The addition of these experimental elements to the software model enhances the accuracy of the simulation.

Before proceeding with the presentation of the system model, there must be some clarification of the nomenclature to be henceforth used. Consider Fig. 2, which shows a simple schematic representation of the actuator.

In Fig. 2, $\dot{m}_A$ and $\dot{m}_B$ represent the net mass flow rates to chambers A and B, respectively, whose pressures and temperatures are given by p_A, T_A and p_B, T_B. F_p is the resultant force due to the pressure differential between the chambers, and is given by:

$$F_p = p_A A_A - p_B A_B - F_{atm} \tag{1}$$

where A_A and A_B are the respective piston areas of chambers A and B, and the force due to atmospheric pressure (p_{atm}) is defined as $F_{atm} = p_{atm} A_r$, where A_r is the actuator rod's cross-sectional area. F_{ext} is any external force and F_{fr} is the friction force. M is the payload mass and $x, \dot{x}, \ddot{x}$ are, respectively, position, velocity and acceleration. Since the servo-valves switch control functions when there is a change in the direction of motion, it is important to establish the definition of forward (FWD) direction as left to right, and backward (BWD) direction as right to left. So that the chambers can be identified based on their role in a control task, it is further defined that:

– **Charging chamber** is the chamber whose volume is increasing during a given movement (e.g., chamber A in a FWD movement).

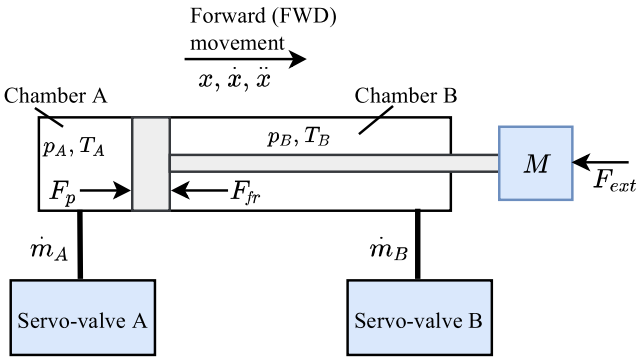

Fig. 2 Schematic representation of the pneumatic actuator

– **Discharging chamber** is the chamber whose volume is decreasing during a given movement (e.g., chamber B in a FWD movement).

2.2 System model

The derivation of the system model herein presented can be found in detail in [36]. For the purpose of this work, a small update to the servo-valve models was made, which will later be detailed.

The mechanical model of the system is given in Eq. 2:

$$\ddot{x} = \frac{F_p - F_{fr} - F_{ext}}{M} \tag{2}$$

where F_p is given by Eq. 1.

For the purpose of this work, it is assumed that there are no external forces acting on the system, and thus $F_{ext} = 0$. The friction force F_{fr} is given by a LuGre friction model [37], the parameters of which were determined in [9] for the actuator discussed in this work. The LuGre model is a dynamic model that captures the Stribeck effect, Coulomb friction, stiction, and viscous friction, therefore predicting the friction phenomena (such as stick-slip motion) that are so important in servo-pneumatic motion control.

Concerning the thermodynamic model of the actuator, the pressure dynamics inside the chambers are described by Eq. 3, where $\gamma = 1.4$ is the specific-heat ratio at ambient temperature, p_0 is an equilibrium pressure, T and V represent temperature and volume, respectively, the mass flow rate entering or leaving each chamber is given by $\dot{m}_{in}$ and $\dot{m}_{out}$, T_{amb} denotes ambient temperature, and T_{in} is the temperature of the air entering the actuator chamber. R is the specific gas constant for air, $A_q(x)$ is the heat-transfer area of the actuator chamber and λ_0 is a heat-transfer coefficient for p_0 and T_0, reference values for pressure and temperature, respectively [5]. The temperature dynamics are given by Eq. 4.

$$\begin{aligned}\frac{dp}{dt} &= -\gamma \frac{p}{V}\frac{dV}{dt} + \gamma \frac{R}{V}\dot{m}_{in} T_{in} - \gamma \frac{R}{V}\dot{m}_{out} T \\ &\quad + \frac{\gamma - 1}{V}\lambda_0 \sqrt{\left(\frac{pT}{p_0 T_0}\right)} A_q(x)(T_{amb} - T)\end{aligned} \tag{3}$$

$$\begin{aligned}\frac{dT}{dt} &= \frac{T}{V}\frac{dV}{dt}(1-\gamma) + \dot{m}_{in}\frac{RT}{Vp}(\gamma T_{in} - T) - \dot{m}_{out}\frac{RT^2}{Vp}(\gamma - 1) \\ &\quad + \frac{(\gamma - 1)T}{pV}\lambda_0 \sqrt{\left(\frac{pT}{p_0 T_0}\right)} A_q(x)(T_{amb} - T)\end{aligned} \tag{4}$$

The servo-valve model is obtained by application of the ISO 6358 standard [38]. Consider the three-way servo-valve represented in Fig. 3.

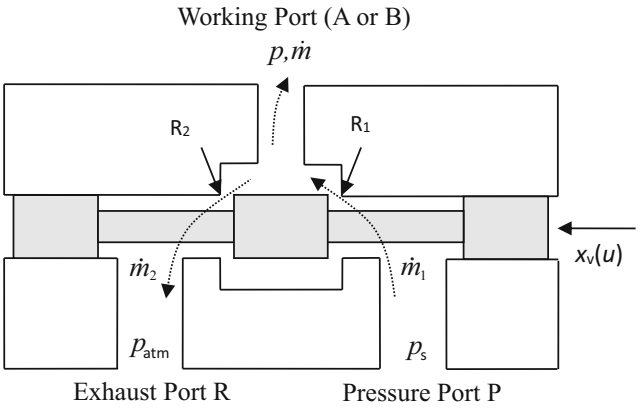

Fig. 3 Schematic representation of a 3-way servo-valve

Port P is connected to the pressure source and Port R to the atmosphere. The working port is connected to an actuator chamber (A or B). The area of orifice R_1 and R_2 varies with the spool position x_v, which is a function of a voltage u (the control action). The spool position x_v is assumed to have a static relationship with the control action u, since the servo-valve dynamics are much faster than the actuator dynamics.

According to ISO 6358, for a given restriction R_i, the mass flow rate through that orifice is given by Eq. 5.

$$\dot{m} = C_i(u)\, p_{ui}\, \rho_0 \sqrt{\frac{293.15}{T_{ui}}}\, Y \tag{5}$$

with Y given by:

$$Y = \begin{cases} 1, & \text{if } \frac{p_{di}}{p_{ui}} \leq r_i(u) \\ \sqrt{1 - \left(\frac{p_{di}/p_{ui} - r_i}{1 - r_i}\right)^2}, & \text{if } \frac{p_{di}}{p_{ui}} > r_i(u) \end{cases} \tag{6}$$

where C_i is the sonic conductance, p_{ui} and p_{di} are, respectively, the upstream and downstream pressures, and r_i is the critical pressure ratio of the valve orifice, below which the flow becomes choked. $C_i(u)$ and $r_i(u)$ are given as functions of u because they vary with the area of the orifice. Their dependence of u was determined experimentally, for the servo-valves simulated in this work, in [8].

Recall Fig. 3, and let $\dot{m}_{ij}$ be the mass flow rate through orifice j of the servo-valve attached to chamber i. The net mass flow rate through the working port (A or B) (Eq. 7) can be obtained from the law of conservation of mass:

$$\dot{m}_{A,B} = \dot{m}_{A1,B1} - \dot{m}_{A2,B2} \tag{7}$$

Finally, the mass flow rate entering or leaving an actuator chamber (A or B) will then be given by Eqs. 8 and 9:

$$\dot{m}_{A,Bin} = \begin{cases} \dot{m}_{A,B} & \text{if } \dot{m}_{A,B} > 0 \\ 0 & \text{if } \dot{m}_{A,B} \leq 0 \end{cases} \tag{8}$$

$$\dot{m}_{A,Bout} = \begin{cases} 0 & \text{if } \dot{m}_{A,B} \geq 0 \\ \dot{m}_{A,B} & \text{if } \dot{m}_{A,B} < 0 \end{cases} \tag{9}$$

As was previously mentioned, an update to the servo-valve model was done during the work herein presented. The model was extended to contemplate reverse-flow in the servo-valve orifices, should the pressure in the actuator chambers rise above p_s or fall under p_{atm}. In Eqs. 5 and 6, upstream (p_{ui}) and downstream (p_{di}) pressure values will depend on the servo-valve orifice and the working conditions. Equations 10–13 specify the upstream and downstream pressures for orifices 1 and 2 in Fig. 3.

$$p_{u1} = \begin{cases} p_s & \text{if } p_s \geq p_{A,B} \\ p_{A,B} & \text{if } p_s < p_{A,B} \end{cases} \tag{10}$$

$$p_{d1} = \begin{cases} p_{A,B} & \text{if } p_s \geq p_{A,B} \\ p_s & \text{if } p_s < p_{A,B} \end{cases} \tag{11}$$

$$p_{u2} = \begin{cases} p_{A,B} & \text{if } p_{A,B} \geq p_{atm} \\ p_{atm} & \text{if } p_{A,B} < p_{atm} \end{cases} \tag{12}$$

$$p_{d2} = \begin{cases} p_{atm} & \text{if } p_{A,B} \geq p_{atm} \\ p_{A,B} & \text{if } p_{A,B} < p_{atm} \end{cases} \tag{13}$$

2.3 Coupling of pressure and velocity

The control architecture presented in this paper features independent control of pressure and motion, but it is easy to see that, in practice, the dynamics relating to those variables are inextricably linked, since pressure differences in the actuator chambers are the driving force through which motion is created—the motion control loop will therefore influence the pressure loop and vice-versa. The understanding of this coupling of dynamics, and how it changes with the system state, can be advantageously used in the control design phase.

Despite this coupling posing a challenge to the independent control of pressure and motion, certain characteristics of the system allow for a decoupling of the aforementioned dynamics. Consider Fig. 4, which, for a forward movement, represents

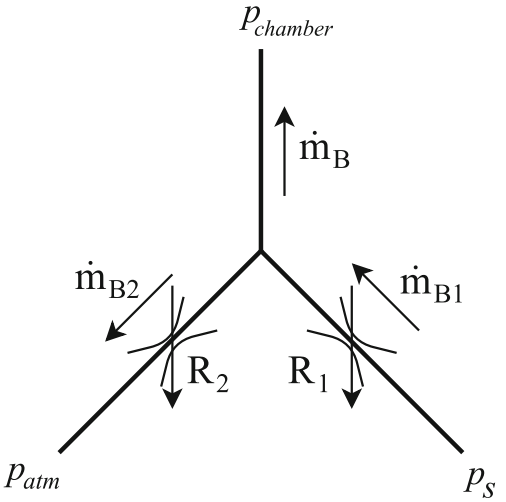

Fig. 4 Schematic representation of the servo-valve restrictions

the orifices of the servo-valve connected to the discharging chamber. The air supply provides air at a constant pressure $p_s = 7$ bar and temperature $T_s = 298.15$ K.

As was already mentioned, the control architecture herein presented aims to have metered-out flow in the discharging chamber, for the sake of motion smoothness. Now consider the classic meter-out configuration, where there is no R_1—there is only a simple flow restrictor limiting the outward flow from the discharging chamber. In that case, there is only R_2 and the net mass flow rate is therefore given simply by $\dot{m}_B = \dot{m}_{B2}$. Using the ideal gas law and the conservation of mass principle, $\dot{m}_B$ can be rewritten as:

$$\dot{m}_B = \rho_B Q_B = \frac{p_B}{RT_B}\dot{x}A_B \tag{14}$$

In Eq. 14, Q_B is the net volumetric flow rate through working port B. Resorting to Eqs. 5 and 14, Eq. 7 can be rewritten as:

$$\frac{p_B}{RT_B}\dot{x}A_B = -C_{B2}p_B\rho_0\sqrt{\frac{293.15}{T_B}} \tag{15}$$

The p_B terms cancel out and thus piston velocity is given by:

$$\dot{x} = -\frac{RT_B}{A_B}C_{B2}\rho_0\sqrt{\frac{293.15}{T_B}} \tag{16}$$

It can be seen that in this case (classic meter-out with one restrictor), having choked flow does indeed result in a steady-state piston velocity that is insensitive to pressure fluctuations in the discharging chamber—this is because choked flow conditions impose a hard limit on the volumetric flow rate, which in turn defines piston velocity. Even when considering the present case of a servo-valve with two orifices (Fig. 4), in a meter-out setting there would ideally exist no flow whatsoever through R_1. However, there is a problem with using a servo-valve—simulation results show what would also be expected in practice: there is always leak flow even when an orifice is nominally closed. This means that one then has $\dot{m}_B = \dot{m}_{B1} - \dot{m}_{B2}$ and thus, following the same procedure used to deduce Eq. 16, piston velocity is now given by:

$$\dot{x} = \frac{RT_B}{A_B}C_{B1}\frac{p_s}{p_B}\rho_0\sqrt{\frac{293.15}{T_s}} - \frac{RT_B}{A_B}C_{B2}\rho_0\sqrt{\frac{293.15}{T_B}} \tag{17}$$

We see that a p_B term has been introduced in the velocity equation—even in choked flow conditions, the steady-state velocity may be affected by pressure fluctuations inside the discharging chamber. To tackle this issue, we can resort to pressure regulation to not only guarantee choked flow, but also to try to keep those pressure fluctuations in check. This combination of choked meter-out flow and constant pressure results in system conditions that are ideal for smooth motion.

3 Independent, linear PID control of pressure and motion

A schematic representation of the control architecture can be seen in Fig 5. In the proposed control architecture, the pressure in the discharging chamber (p_B in a FWD movement) is fed back to the pressure controller, which is actually connected to the charging chamber's servo-valve. This servo-valve acts so as to maintain the pressure in the discharging chamber (p_{dch}) at a constant value, thus acting like a regulator. The other servo-valve, connected to the discharging chamber, acts according to the motion specifications of velocity and position. In steady-state conditions, it essentially tries to emulate a sort of meter-out configuration, limiting the flow rate of air exiting the discharging chamber and thus controlling piston velocity. This

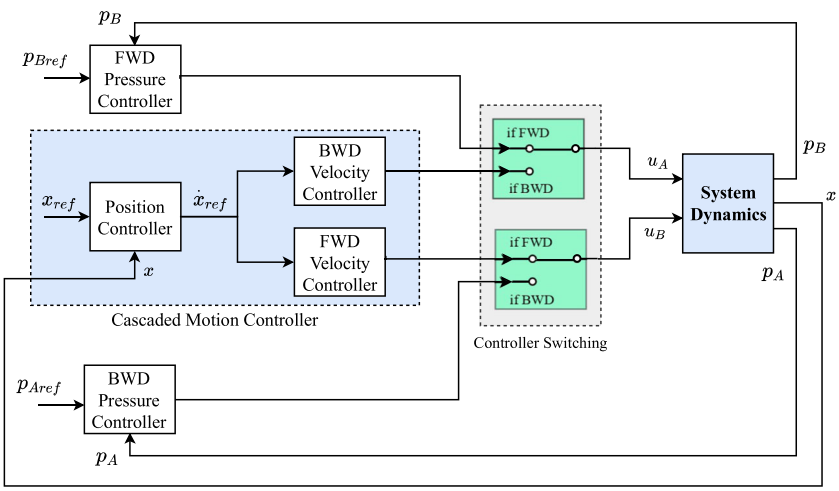

Fig. 5 Simplified schematic representation of the control architecture

velocity controller is part of a cascaded motion controller—the input of the velocity controller is the output of a proportional positioning controller.

Both control loops (pressure and motion) rely on linear PID-family controllers to impose the desired dynamics, for the reasons presented at the end of the introduction.

3.1 Pressure control

The pressure control-loop aims to indirectly control the pressure in the discharging chamber. For a FWD movement, this means controlling p_B by using servo-valve A to act on p_A. The controller essentially acts as a regulator, trying to maintain pressure at a constant value of $p_{dch} = 3\ bar$, while of course still allowing the pressure variations needed for the system to present satisfactory dynamic behaviour. Therefore, the requirements on pressure control are not very strict—the ultimate goal of the overall control system is to provide accurate, smooth motion control.

The first thing to discuss in the control design process is the aforementioned pressure reference of $p_{dch} = 3\ bar$. This value is chosen because it poses as a good middle-ground between p_{atm} and p_s, as the pressure ratios will generally lie under the critical pressure ratio (around 0.5 [8]), promoting choked flow and its underlying advantages for motion control.

It should then be made clear what specifications the pressure controller should meet. As was already said, they are not very strict—the controller should be able to bring p_{dch} relatively quickly to a steady-state 3 bar value and, once the desired position is achieved (with a given error), it should be able to compensate for natural pressure dynamics that would otherwise displace the piston after it has already stopped.

The designed pressure control-loop is built around a simple PI controller with a velocity reference feed-forward term, which was introduced due to the knowledge of the coupling between pressure and velocity. It is known that, for a FWD movement, if the motion controller requests a decrease in velocity, then servo-valve B is going to act so as to increase p_B to brake piston momentum. This information can be used and fed directly to the pressure controller, anticipating the system's dynamic response. Having a PI pressure regulator with this feed-forward term, two main problems were addressed by the introduction of new control action terms:

- The appearance of hunting limit-cycles in positioning tasks, due to the non-linear nature of friction associated with the integral control action. This was solved by implementing an integrator freeze as a function of positioning error: while the positioning error remains smaller than a pre-defined value, the output of the integrator will be held constant and equal to its value at the instant it entered the freeze-zone.
- The *sticking and restarting phenomenon* (SRP) [39], a problem that arises due to unobserved pressure dynamics. A solution was found by introducing a control action term that was proportional to the pressure in the charging chamber.

An anti-windup mechanism [40] was also implemented. The final pressure controller is exemplified for FWD motion in Fig. 6.

For the sake of clarity concerning the integrator freeze, the control action equations (Eqs. 18–19) for the different working conditions are presented. Let ε_x be the positioning error, and u_{frz} the integral control action value at the instant in which the system enters the integrator freeze-zone. u_{int} is the integral control action, u_{pch} is the control action proportional to the pressure in the charging chamber, u_P is the usual proportional control action and u_{FF} is the velocity reference feed-forward term.

The pressure-loop control action will then be given, for FWD motion, by:

If $|\varepsilon_x| \geq 0.5$ mm:

$$u_A(t) = u_{int}(t) + u_{pch}(t) + u_P(t) + u_{FF}(t) \tag{18}$$

If $|\varepsilon_x| < 0.5$ mm :

$$u_A(t) = u_{frz} + u_{pch}(t) + u_P(t) + u_{FF}(t) \tag{19}$$

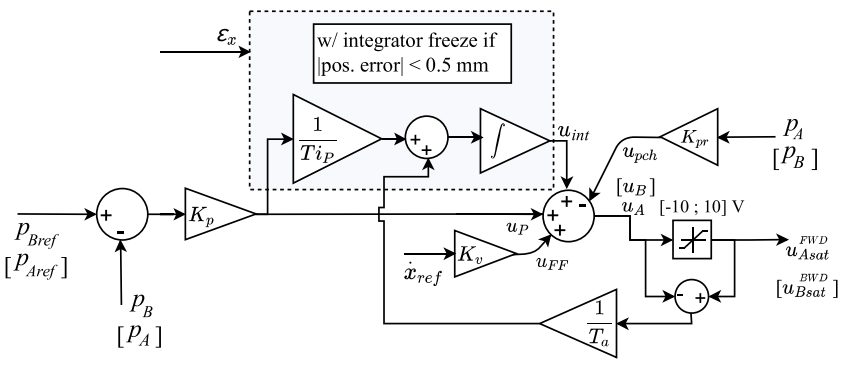

Fig. 6 Schematic representation of the pressure controller for FWD / [BWD] motion

3.2 Motion control

A schematic representation of the cascaded motion controller can be seen in Fig. 7. Recall that the velocity and acceleration values are estimated by a Kalman filter, since only the piston position is available.

The motion and pressure controllers were essentially developed in parallel, and so the solutions to major motion control problems that originated in the pressure control loop have already been discussed, namely the hunting limit-cycles and the SRP phenomenon.

The motion control-loop is composed of a velocity controller in cascade with a proportional position controller. The velocity controller includes a derivative term implemented with an observed acceleration feedback, in order to provide damping action. This P-D velocity controller with a P-only position controller (in tandem with the final pressure controller) presented satisfactory positioning results, with acceptable steady-state errors and smooth movements, in response to S-shaped (sigmoid) inputs. However, to increase robustness to payload mass variations, a new control term was introduced, proportional to the pressure error ($\varepsilon_{pdch} = p_{ref} - p_{dch}$). The attempt to implement this term was inspired by the earlier coupling discussion, and it further proves that even a qualitative understanding of the interacting dynamics of pressure and velocity allows for the successful use of pressure information in the velocity controller (and vice-versa).

3.3 Controller switching

With the present control architecture, the servo-valve controllers should switch roles when the direction of motion is changed. It was therefore necessary to define a controller switching strategy. The implemented strategy consists in simply evaluating the sign of the velocity reference. This strategy can be summarized in Algorithm 1, and refers to the total control actions specified in Figs. 6 and 7.

Algorithm 1: Active controller depends on sign of $\dot{x}_{ref}$

```
function u_A, u_B (ẋ_ref)
if ẋ_ref ≥ 0 then
    u_A = u_Asat^FWD;   // FWD Pressure Control
    u_B = u_Bsat^FWD;   // FWD Motion Control
else
    u_A = u_Asat^BWD;   // BWD Motion Control
    u_B = u_Bsat^BWD;   // BWD Pressure Control
end
```

At start-up, Algorithm 1 is initialized with the initial $\dot{x}_{ref}$ value, and the initial conditions of the integrators in the pressure controllers (FWD and BWD) are set to 0.

Concerning the switching per se, an effort was made for it to happen as smoothly as possible. Ideally, a bump-less switching could be implemented that guaranteed that the control action of the new controller would be initialized at the same value of the previous one. In practice, this would be achieved by continually resetting the integrator of the inactive controller and setting a dynamic initial condition. This way, when switching happens the resetting will stop and the controller will start up with the right control action. However, the velocity controller has no integrator—it was therefore only possible to smooth the transition from velocity control to pressure control. For a smooth transition to happen, the total pressure control action ($u_{pressure}$) should equal the total velocity control action ($u_{velocity}$). Equation 20 specifies the equality that should then be verified at the moment of switching.

$$\begin{aligned} & u_{pressure} = u_{velocity} \\ \Leftrightarrow\ & u_{int} + u_P + u_{FF} + u_{pch} = u_{velocity} \end{aligned} \tag{20}$$

where, recalling the terms of the pressure controller, u_{int} is the integral term, u_P is the proportional term, u_{FF} is the velocity feed-forward term and u_{pch} is a term proportional to the pressure in the charging chamber. Since the pressure integrator can be fed a continually updated initial condition, a simple manipulation of Eq. 20 gives the value which that initial condition must take:

$$u_{int} = u_{velocity} - (u_P + u_{FF} + u_{pch}) \tag{21}$$

Concerning the pressure to velocity transition, which cannot be forced to happen smoothly, it should be noted that it is not problematic at all for S-curve inputs. When the piston is stationary at a given position, the pressure control action is in its equilibrium value. When a new reference is given that requires a controller switch, the velocity controller kicks in with all null terms (for S-curve inputs), except for the pressure error (ε_{pdch}) term. Therefore, for an S-curve input, at the instant of switching, the difference between the total velocity and pressure control actions is given simply by Eq. 22:

$$u_{velocity} - u_{pressure} = K_{ep}\varepsilon_{pdch} \tag{22}$$

Since the K_{ep} gain is relatively small, there is only a small discontinuity in the control action, which was seen to have no noticeable effects on performance. The final controller, with both pressure and motion control-loops, can be seen in Fig. 8.

4 Results

Some results will now be presented, obtained both through simulation of the system and experimental tests. The software implementation of the control architecture and system

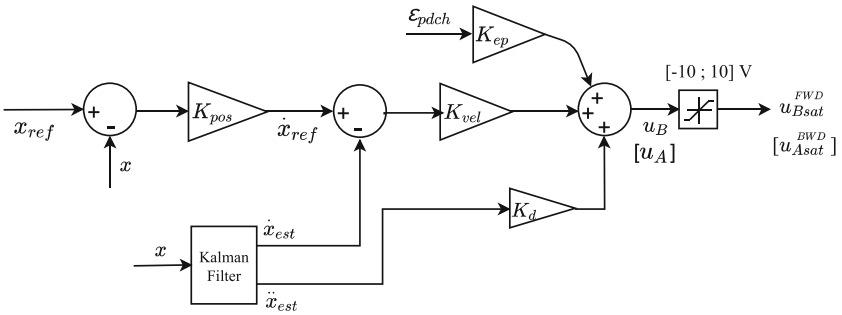

Fig. 7 Schematic representation of the motion controller for FWD / [BWD] motion

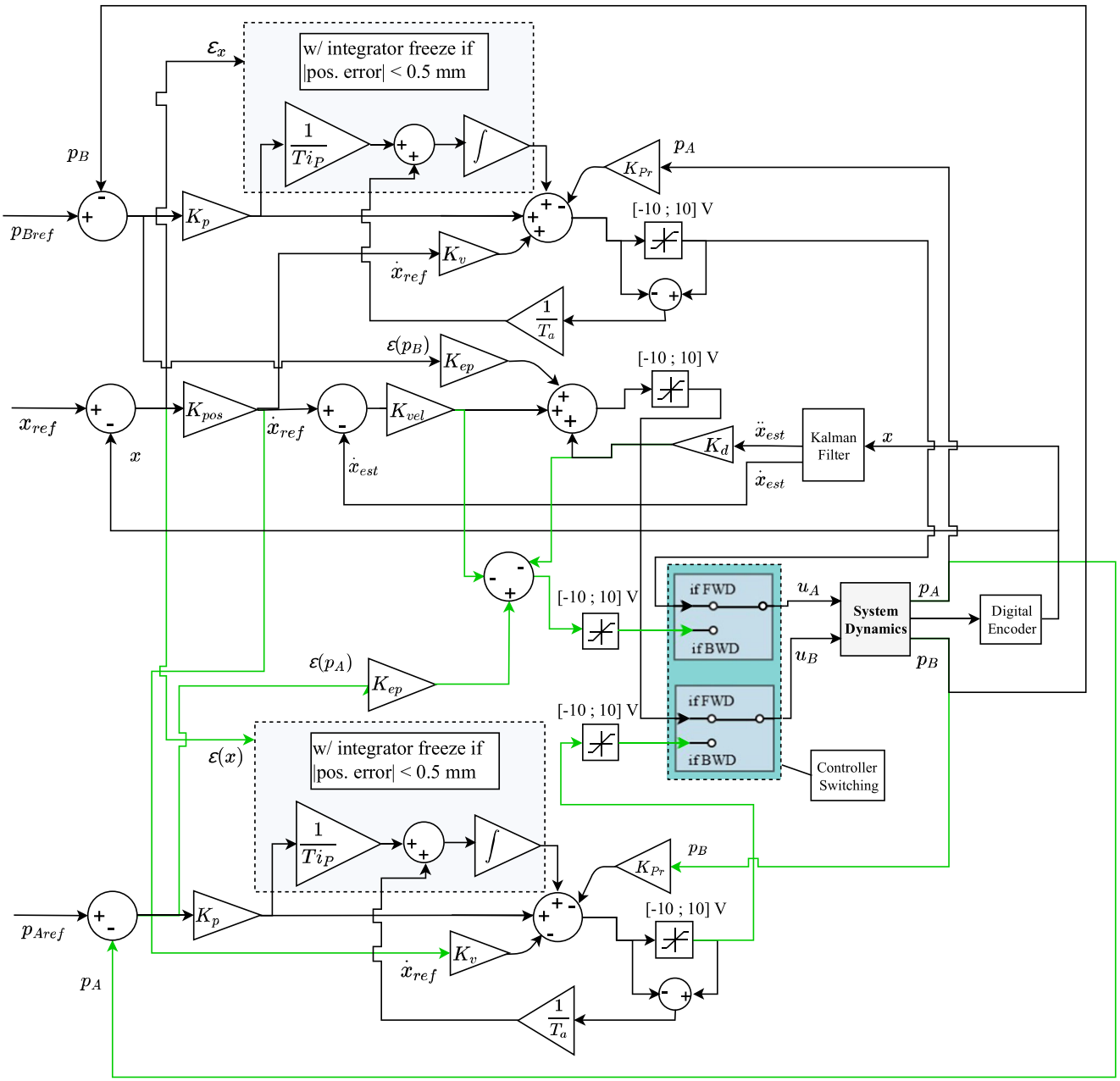

Fig. 8 Final control scheme. Green lines relate to the backward controller (BWD)

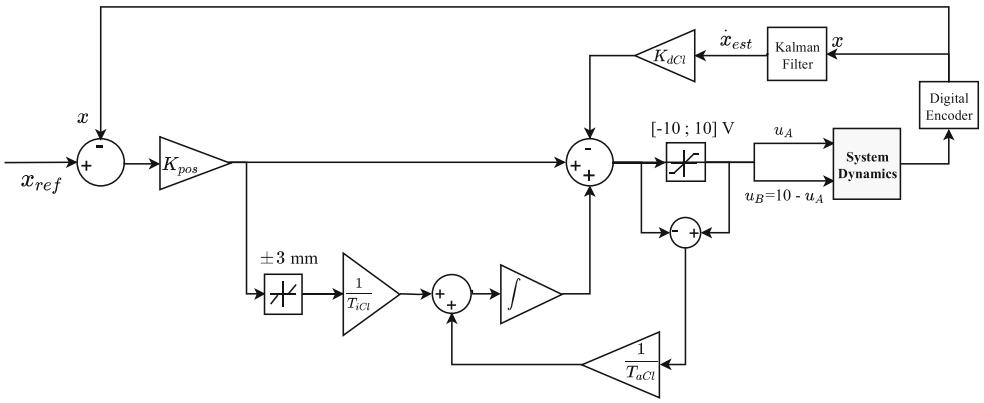

Fig. 9 Classical architecture PID controller

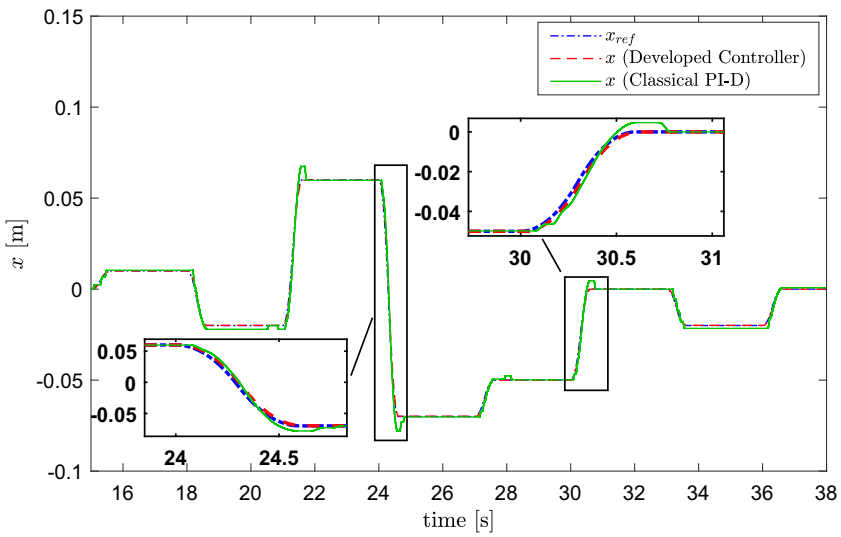

Fig. 10 Simulated response to S-curve inputs, $m = 3$ kg

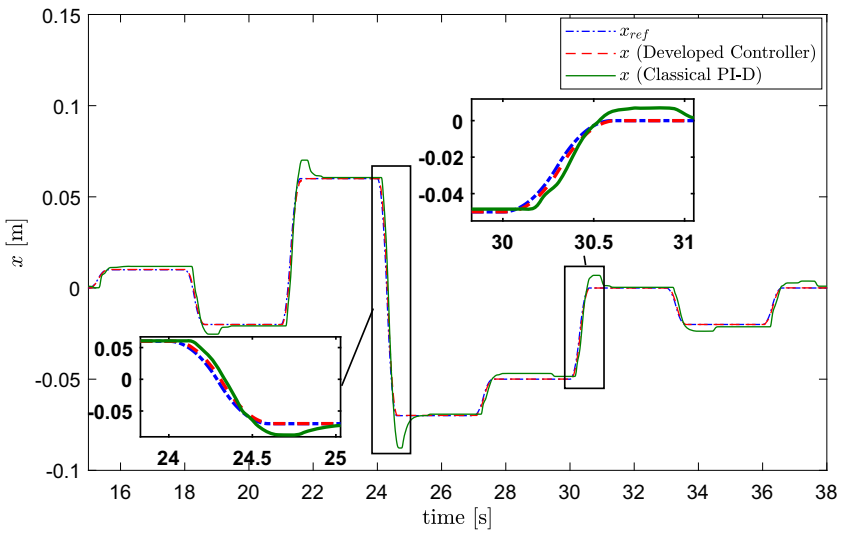

Fig. 11 Experimental response to S-curve inputs, $m = 3$ kg

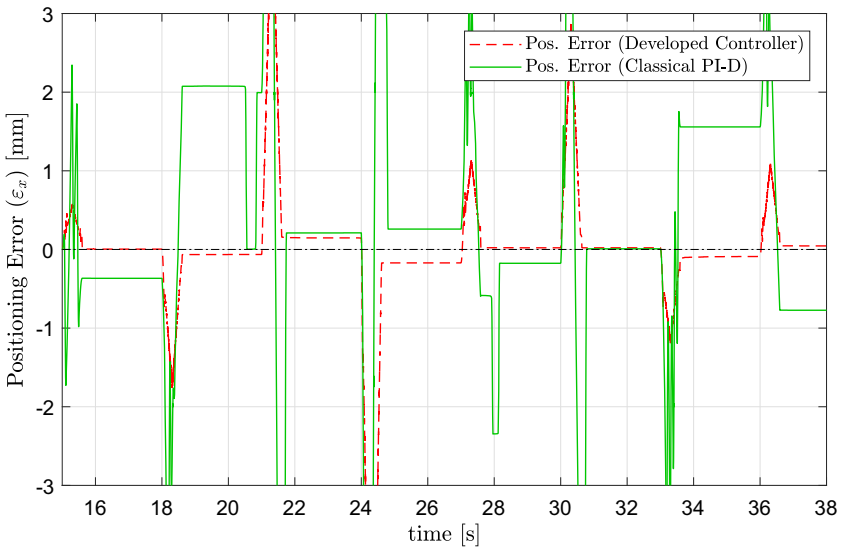

Fig. 12 Positioning error for S-curve response in Fig. 10

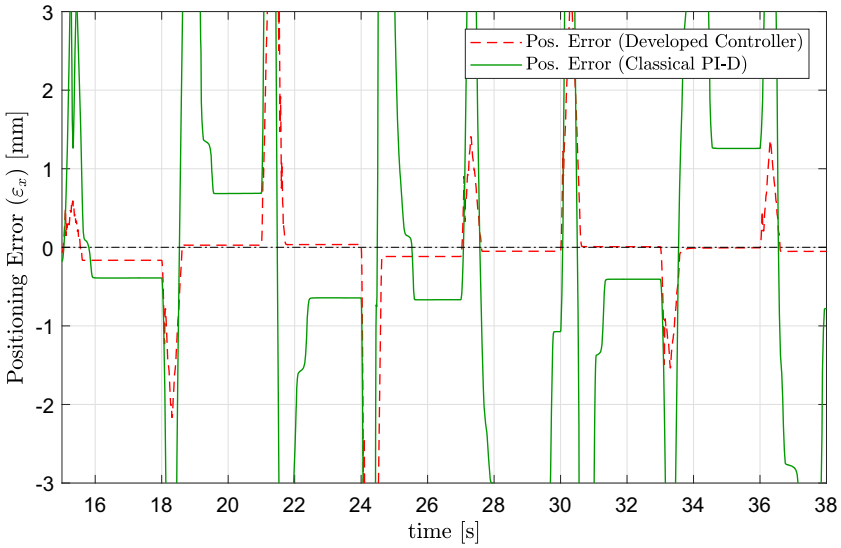

Fig. 13 Positioning error for S-curve response in Fig. 11

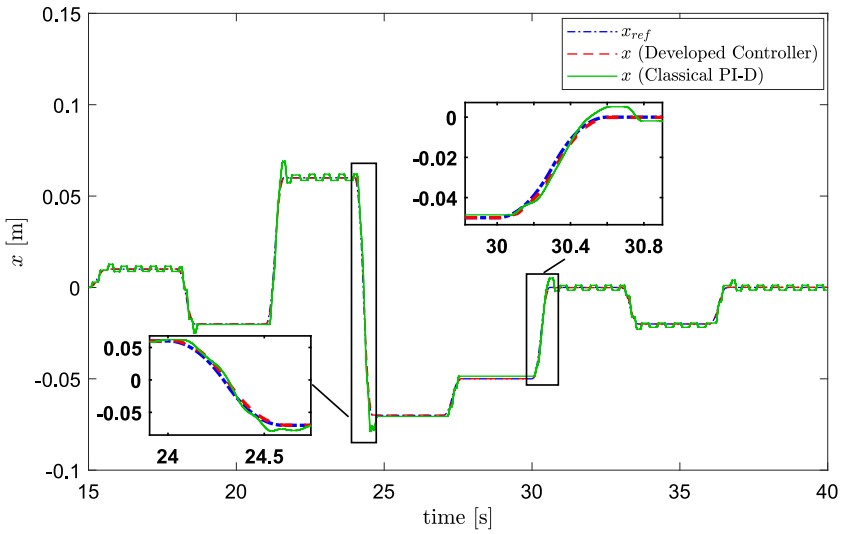

Fig. 14 Simulated response to S-curve inputs, $m = 8$ kg

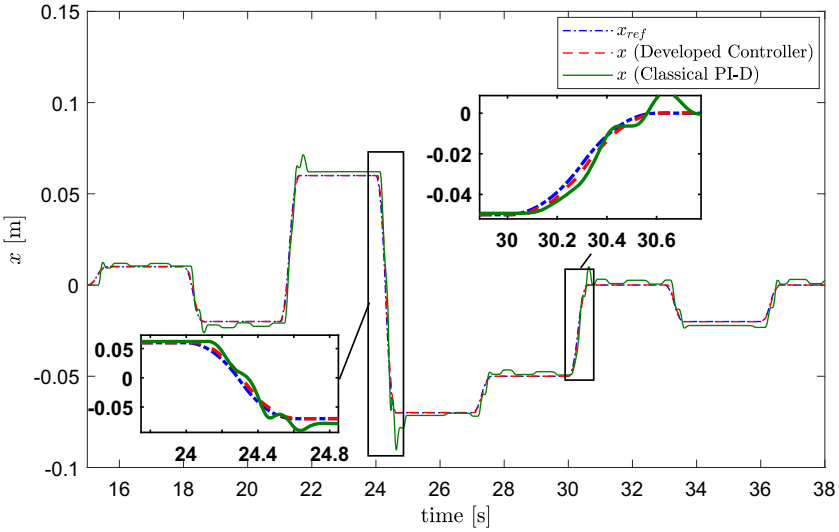

Fig. 15 Experimental response to S-curve inputs, $m = 8$ kg

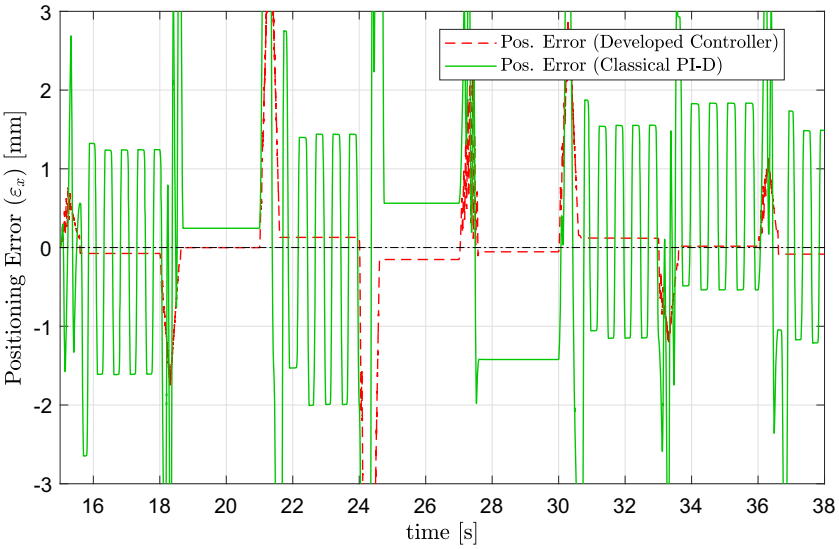

Fig. 16 Positioning error for S-curve response in Fig. 14

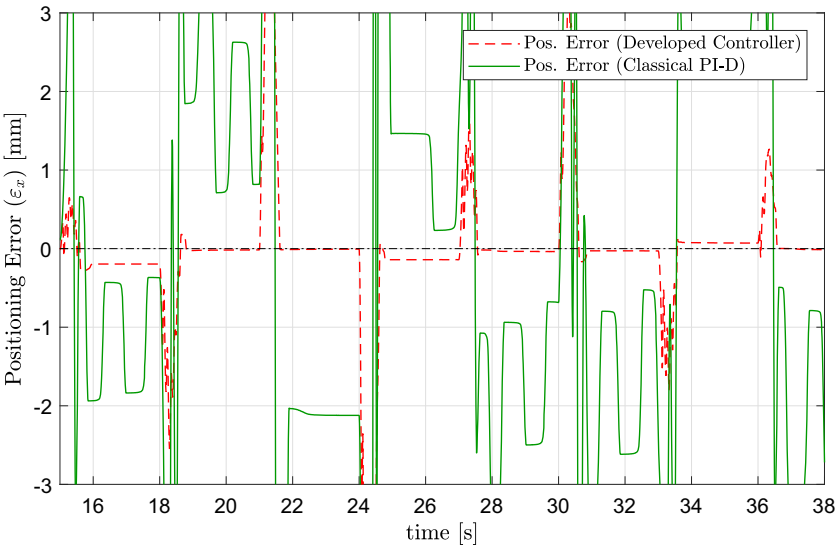

Fig. 17 Positioning error for S-curve response in Fig. 15

Table 1 Controller parameters

Controller	K_p	K_v	K_{pr}	T_a	T_{ip}	K_{pos}	K_{vel}	K_d	K_{ep}	K_{dCl}	T_{iCl}	T_{aCl}
Class. PID	–	–	–	–	–	130	–	–	–	0.7	0.07	0.04
New Controller	2×10^{-5}	10	2×10^{-5}	0.04	0.09	40	80	0.6	3×10^{-5}	–	–	–

model was done in MATLAB/*Simulink*®. The ODE23s (stiff/Rosenbrock) solver was used due to numerical stiffness in the LuGre friction model, and a variable step-size was used. The experimental implementation was done by setting up a *Real-Time Windows Target* in *Simulink*®, using a fixed-step solver (ODE3 Bogacki-Shampine) with step-size equal to the sampling frequency of the data acquisition system (1 kHz). (For the open-loop characterization of the system model, see [36].)

The performance of the newly developed controllers is compared with that of a classical PID-family controller with symmetrical control actions ($u_A = -u_B$). The datum controller for this comparison was a PI-D [41] with a dead-zone in the integrator to avoid limit-cycles due to the combination of friction and integral action [42]. An anti-windup mechanism (Fig. 9) was also included. Some effort was put into the experimental tuning of this controller, so that the comparison could be as fair as possible. Given the dead-zone in the integrator, a high proportional gain was necessary to reduce steady-state errors, albeit leading to larger overshoots.

The results show the performance of the controllers for positioning tasks with step inputs and S-shaped inputs. The latter is given more focus, as it is important that the controller be able to follow the general shape of the S-shaped reference curve, as that implies smooth motion.

Figs. 10, 11, 12, 13, 14, 15, 16, and 17 show the system's simulated and experimental response to S-curve inputs of different amplitudes, with 0.6 s reaching time. This was done for different values of the payload (3 and 8 kg). Controller parameters were experimentally tuned with the aim of finding a universal tuning that presented good dynamic response and was robust to payload mass variations between 3 and 8 kg. It should be mentioned that the best tuning found in the simulation environment was very close to the final experimental tuning, further validating the software model as a preliminary design tool. This tuning (presented in Table 1) works for both forward and backward motion, reducing the tunable parameters in half and simplifying the tuning process. It also works for both step-inputs and S-shaped inputs, although it should be noted that it favors the latter (S-curves). Since motion smoothness was considered one of the main objectives, attention was focused on the S-shaped input response—recall that such an input also significantly smooths out the transition between the pressure and velocity controllers. Notwithstanding, and for the sake of generality, the experimental closed-loop step-response is also presented in Figs. 18, 19, 20, and 21 and.

Analysis of the results shows that, for an S-shaped input, the newly developed controller is able to smoothly move the piston from any point to another in under 0.6 seconds and in, generally, one swift motion, with no overshoot, and with acceptable steady-state positioning errors ($\varepsilon_{ss} < 0.2$ mm). Furthermore, it maintains satisfactory performance when adding 5 kg to the payload, which is not true for the classical

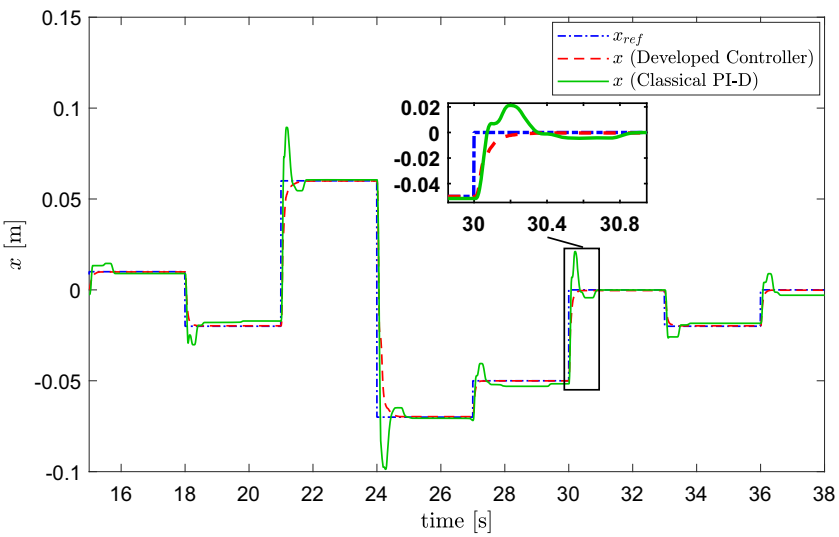

Fig. 18 Experimental response to step-inputs, $m = 3$ kg

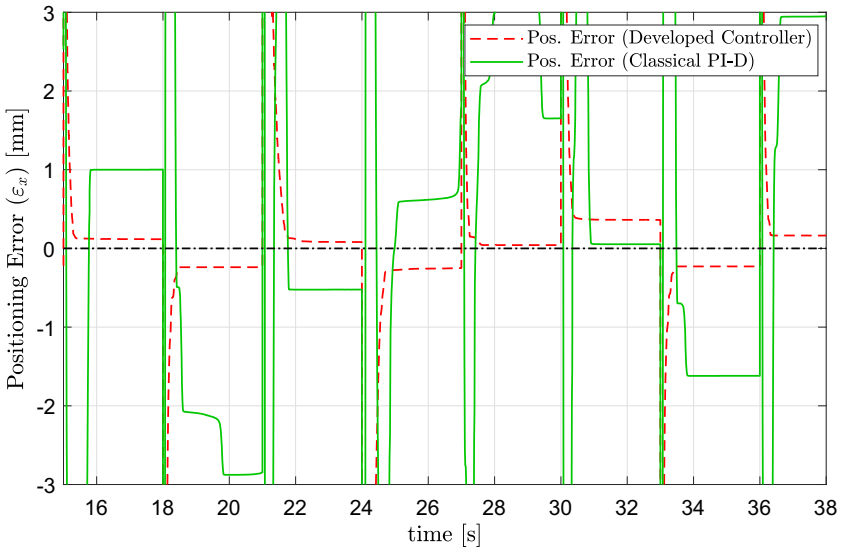

Fig. 19 Positioning error for the step-response in Fig. 18

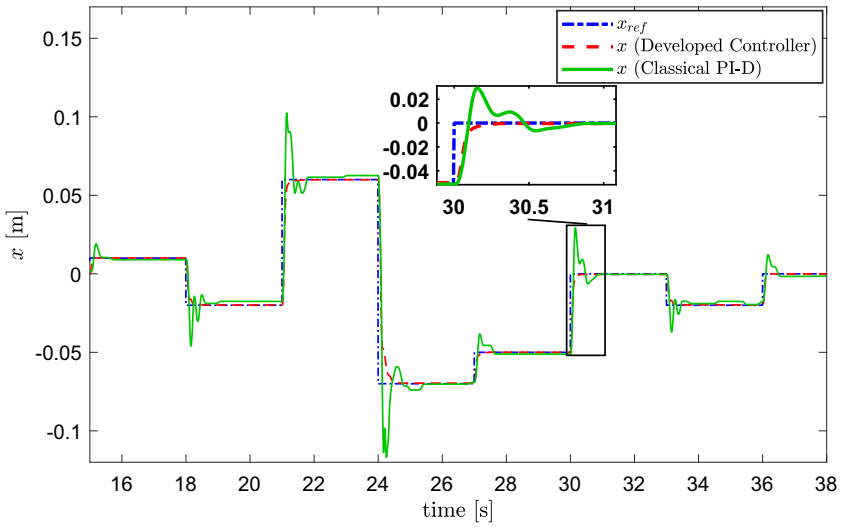

Fig. 20 Experimental response to step-inputs, $m = 8$ kg

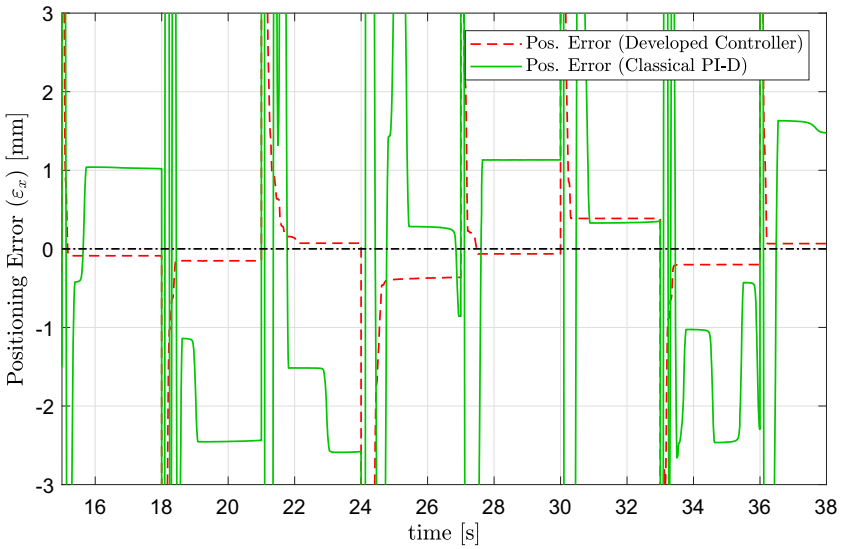

Fig. 21 Positioning error for the step-response in Fig. 20

Table 2 Performance metrics for S-curve inputs for simulated and experimental tests, with variable payload mass m

	Controller	Max. % Overshoot	Max. ε_{ss} (mm)
$m = 3$ kg	Class. PID	9.2%	2.07
(Sim.)	New Controller	–	0.17
$m = 3$ kg	Class. PID	13.6%	1.25
(Exp.)	New Controller	–	0.17
$m = 8$ kg	Class. PID (*)	16.6%	1.42
(Sim.)	New Controller	–	0.16
$m = 8$ kg	Class. PID (*)	20%	2.12
(Exp.)	New Controller	0.4%	0.20

The (*) symbol means undesired oscillations were observed

PID, for which hunting limit-cycles start to appear. For the harsher step-inputs, the developed controller continues to clearly out-perform the classical one, both in terms of the transient response and steady-state error. The new controller is still able to assure that no overshoot occurs, and the movements remain relatively smooth. Even though the rise time of the classical controller is smaller, the oscillations in its response make for larger settling times—the developed controller can therefore actually settle faster than the classical one.

Table 2 sums up the performance metrics for the positioning tasks of Figs. 10, 11, 12, 13, 14, 15, 16, and 17, while Table 3 presents the relevant step-response metrics for Figs. 18, 19, 20, and 21, where the time-related metrics are given for a 130-mm step-input.

The experimental results also seem to ascertain the quality of the model as a powerful tool for early-stage control design, as it seems able to predict stick-slip motion and the appearance of limit-cycles, two difficult friction-related phenomena. With this, the control engineer is able to efficiently evaluate the potential of a control law in overcoming those problems, while running quick simulations as opposed to more cumbersome, expensive and time-consuming experimental tests, which may be unnecessary in the early stages of the control design.

5 Conclusions

At the core of this work was the development of a two servo-valve control architecture for independent motion and pressure control of a servo-pneumatic system. The aim was to achieve smooth motion and accurate positioning through use of linear PID-family controllers—one for each servo-valve. The one connected to the charging chamber regulates pressure in the discharging chamber (with a 3 bar reference value), while the other handles motion specifications. The pressure regulator helps in shielding piston velocity from being affected by pressure fluctuations in the discharging chamber, since it not only tries to keep constant pressure, it does so at a value that guarantees choked flow, therefore making the volumetric flow rate independent of pressure and promoting motion smoothness. The pressure loop features a PI controller with a $\dot{x}_{ref}$ feed-forward term, a term that is proportional to the pressure in the main chamber, and an integrator freeze mechanism. The motion controller features a P-D velocity controller with a pressure error (ε_{pdch}) term, in cascade with a P-only positioning controller.

Both simulation and experimental results show that the controller developed in this work presents virtually no overshoot, features robustness to payload variations and is able to impose smooth movements between positions, with most of them being completed in one swift motion. It is also easy to see that it fares quite well against a classical PID controller—for an S-shaped input (which promotes motion smoothness) maximum steady-state errors were 0.2 mm for the developed controller *vs* 2.12 mm for the classical PID. It should however be noted that the latter controller has a 3-mm dead-zone in the integrator to avoid limit-cycles, and this contributes to the large steady-state errors.

Overall, experimental results are in agreement with those obtained through simulation and seem to validate the new control architecture, as it meets the qualitative requirements that were initially set: smooth movement between positions with acceptable steady-state positioning errors. The main difficulty in the implementation of the new control strategy lies in the large number of controller parameters, which can

Table 3 Performance metrics for the closed-loop step-response, with variable payload mass m

	Controller	Max. % overshoot	Max. ε_{ss} (mm)	t_r (s)	t_p (s)	t_s (s)
$m = 3$ kg	Class. PID	42.20%	2.88	0.08	0.28	0.83
(Exp)	New controller	–	0.36	0.19	–	0.44
$m = 8$ kg	Class. PID (*)	53.13%	2.44	0.07	0.26	1.32
(Exp.)	New controller	–	0.38	0.20	–	0.40

Rise time t_r is defined as the time it takes for the response to rise from 10% to 90% of the steady-state response

Peak time t_p is defined as the time it takes for the response to rise to its peak

Settling time t_s is defined as the time it takes for $|x - x_{ss}|$ to fall to within 2% of x_{ss}

The (*) symbol means undesired oscillations were observed

increase the complexity of the tuning process. However, the fact that a tuning for forward motion works very well for backward motion cuts the number of tunable parameters in half, simplifying the process. Future works will test other types of linear controllers (e.g., state-feedback) within the same control architecture. Other strategies, such as gain scheduling or fuzzy control, would allow the controller parameters to adapt to changing conditions, e.g., very different response times of the two chambers due to big differences in volume, when the piston is close to one of the ends of the cylinder. A more in-depth analysis on the influence of each controller parameter on closed-loop performance would also possibly lead to a more refined tuning and an improvement in performance.

Funding information The authors gratefully acknowledge the funding of Project NORTE-01-0145-FEDER-000022 - SciTech - Science and Technology for Competitive and Sustainable Industries, co-financed by Programa Operacional Regional do Norte (NORTE2020), through Fundo Europeu de Desenvolvimento Regional (FEDER).

References

1. Fujita T, Sakaki K, Makino F, Kikuchi T, Kagawa T, Kawashima K (2002) Accurate positioning of a pneumatic servo system with air bearings. In: Proceedings of the JFPS international symposium on fluid power, (5–3), pp 693–698
2. Wang Y, Su H, Harrington K, Fischer G (2010) Sliding mode control of piezoelectric valve regulated pneumatic actuator for mri-compatible robotic intervention. In: ASME 2010 dynamic systems and control conference, DSCC2010, vol 2, pp 23–28
3. Le MQ, Pham MT, Tavakoli M, Moreau R (2011) Sliding mode control of a pneumatic haptic teleoperation system with on/off solenoid valves. In: 2011 IEEE international conference on robotics and automation, pp 874–879
4. Zhang J-F, Yang C-J, Chen Y, Zhang Y, Dong Y-M (2008) Modeling and control of a curved pneumatic muscle actuator for wearable elbow exoskeleton. Mechatronics 18(8):448–457
5. Falcão Carneiro J, Gomes de Almeida F (2006) Reduced-order thermodynamic models for servo-pneumatic actuator chambers. Proc Inst Mech Eng, Part I: J Syst Control Eng 220(4):301–314
6. Mehmood A, Laghrouche S, El Bagdouri M (2013) Nonlinear dynamic modeling of an electro-pneumatic pressure converter for vgt pneumatic actuator. Int J Autom Technol 14(6):941–953
7. Thomasset D, Scavarda S, Sesmat S, Belgharbi M (1999) Analytical model of the flow stage of a pneumatic servo-distributor for simulation and nonlinear control. In: Proceedings of the sixth Scandinavian international conference on fluid power. Tampere, Finland, May 26–28 1999, vol 3, pp 848–860
8. Falcão Carneiro J, Gomes de Almeida F (2011) Pneumatic servo valve models based on artificial neural networks. Proc Inst Mech Eng Part I: J Syst Control Eng 225(3):393–411
9. Carneiro JF, Gomes de Almeida F (2015) Lugre friction model: application to a pneumatic actuated system. In: Moreira AP, Matos A, Veiga G (eds) CONTROLO'2014—proceedings of the 11th Portuguese conference on automatic control. Springer International Publishing, pp 459–468
10. Mehmood A, Laghrouche S, El Bagdouri M, Ahmed FS (2010) Sensitivity analysis of lugre friction model for pneumatic actuator control. In: 2010 IEEE vehicle power and propulsion conference, pp 1–6
11. Rad C-R, Hancu O (2017) An improved nonlinear modeling and identification methodology of a servo-pneumatic actuating system with complex internal design for high-accuracy motion control applications. Simul Model Pract Theory 75:29–47
12. Saleem A, Taha B, Tutunji T, Al-Qaisia A (2015) Identification and cascade control of servo-pneumatic system using particle swarm optimization. Simul Model Pract Theory 52:164–179
13. Saleem A, Wong CB, Pu J, Moore PR (2009) Mixed-reality environment for frictional parameters identification in servo-pneumatic system. Simul Model Pract Theory 17(10):1575–1586
14. Falcão Carneiro J, Gomes de Almeida F (2012) A macro-micro motion servopneumatic device. Proc Inst Mech Eng I: J Syst Control Eng 226(6):775–786
15. Falcão Carneiro J, Gomes de Almeida F (2012) A high-accuracy trajectory following controller for pneumatic devices. Int J Adv Manuf Technol 61(1):253–267
16. Falcão Carneiro J, Gomes de Almeida F (2014) Micro tracking and positioning using off-the-shelf servopneumatics. Robot Comput-Integr Manuf 30(3):244–255
17. Falcão Carneiro J, Gomes de Almeida F (2015) Accurate motion control of a servopneumatic system using integral sliding mode control. Int J Adv Manuf Technol 77(9):1533–1548
18. Rao Z, Bone GM (2008) Nonlinear modeling and control of servo pneumatic actuators. IEEE Trans Control Syst Technol 16(3):562–569
19. Sorli M, Gastaldi L (2009) Thermic influence on the dynamics of pneumatic servosystems. J Dyn Syst Meas Control 131(2):024501
20. Falcão Carneiro J, Gomes de Almeida F (2013) Using two servovalves to improve pneumatic force control in industrial cylinders. Int J Adv Manuf Technol 66(1):283–301
21. Smaoui M, Brun X, Thomasset D (2005) A combined first and second order sliding mode approach for position and pressure control of an electropneumatic system. In: Proceedings of the 2005, American control conference 2005, vol 5, pp 3007–3012
22. Girin A, Plestan F, Brun X, Glumineau A (2009) High-order sliding-mode controllers of an electropneumatic actuator: application to an aeronautic benchmark. IEEE Trans Control Syst Technol 17(3):633–645
23. Slotine J-JE, Li W (1990) Applied nonlinear control. Prentice Hall, Englewood Cliffs
24. Ning S, Bone GM (2002) High steady-state accuracy pneumatic servo positioning system with pva/pv control and friction compensation. In: Proceedings 2002 IEEE international conference on robotics and automation (Cat. No.02CH37292), vol 3, pp 2824–2829
25. Fok SC, Ong EK (1999) Position control and repeatability of a pneumatic rodless cylinder system for continuous positioning. Robot Comput Integr Manuf 15(5):365–371
26. Situm Z, Pavkovic D, Novakovic B (2004) Servo pneumatic position control using fuzzy PID gain scheduling. J Dyn Syst Meas Control 126(2):376–387
27. Salim SNS, Rahmat MF, Faudzi AMA, Ismail ZH, Sunar N (2013) Position control of pneumatic actuator using self-regulation non-linear PID. Math Probl Eng, vol 2014. https://www.hindawi.com/journals/mpe/2014/957041/cta/
28. Chiou J-S, Tsai S-H, Liu M-T (2012) A PSO-based adaptive fuzzy PID-controllers. Simul Model Pract Theory 26:49–59
29. Chang W-D (2013) Nonlinear CSTR control system design using an artificial bee colony algorithm. Simul Model Pract Theory 31:1–9

30. Stojanovic V, Nedic N (2015) Robust identification of oe model with constrained output using optimal input design. J Frankl Inst 353:576–593
31. Stojanovic V, Filipovic V (2014) Adaptive input design for identification of output error model with constrained output. Circ Syst Signal Process 33(1):97–113
32. Filipovic V, Nedic N, Stojanovic V (2011) Robust identification of pneumatic servo actuators in the real situations. Forsch Ingenieurwes 75(4):183–196
33. Stojanovic V, Nedic N, Prsic D, Dubonjic L, Djordjevic V (2016) Application of cuckoo search algorithm to constrained control problem of a parallel robot platform. Int J Adv Manuf Technol 87(9):2497–2507
34. Pršić D, Nedić N, Stojanović V (2017) A nature inspired optimal control of pneumatic-driven parallel robot platform. Proc Inst Mech Eng C J Mech Eng Sci 231(1):59–71
35. Falcão Carneiro J, Gomes de Almeida F (2016) On the influence of velocity and acceleration estimators on a servopneumatic system behaviour. IEEE Access 4:6541–6553
36. Carneiro J, Almeida Fernando (2012) A neural network based nonlinear model of a servopneumatic system. J Dyn Syst Meas Control 134:024502
37. Canudas de Wit C, Olsson H, Astrom KJ, Lischinsky P (1995) A new model for control of systems with friction. IEEE Trans Autom Control 40(3):419–425
38. ISO 6358 (1989) Pneumatic fluid power—components using compressible fluids—determination of flow-rate characteristics. International Society for Standardization (ISO), Geneva
39. Brun X, Sesmat S, Thomasset D (2005) Study of sticking and restarting phenomenon in electropneumatic positioning systems. J Dyn Syst Meas Control 127(1):173–184
40. Åström KJ, Hägglund T (1995) PID controllers: theory, design, and tuning. Isa Research, Triangle Park
41. Ogata K (2001) Modern control engineering, 4th edn. Prentice Hall PTR, Upper Saddle River
42. Carneiro JF, Gomes de Almeida F (2011) Undesired oscillations in pneumatic systems. Springer, Netherlands, pp 229–243